Journal of Nuclear Materials 377 (2008) 506–521

Contents lists available at ScienceDirect

Journal of Nuclear Materials

journal homepage: www.elsevier.com/locate/jnucmat

Safe radioisotope thermoelectric generators and heat sources for space applications

R.C. O'Brien [a,*], R.M. Ambrosi [a], N.P. Bannister [a], S.D. Howe [b], H.V. Atkinson [c]

[a] University of Leicester Space Research Centre, University Road, Leicester LE1 7RH, UK
[b] Center for Space Nuclear Research, Idaho National Laboratory, ID 83415-3855, USA
[c] University of Leicester Department of Engineering, University Road, Leicester, LE1 7RH, UK

ARTICLE INFO

Article history:
Received 10 February 2008
Accepted 17 April 2008

PACS:
07.77.−n
07.87.+V
21.60.Ka
23.60.+e
24.10.Lx
25.85.Ca
28.90.+i

ABSTRACT

Several isotopes are examined as alternatives to ^{238}Pu that is traditionally used in radioisotope thermoelectric generators (RTGs) and heating units (RHUs). The radioisotopes discussed include ^{241}Am, ^{208}Po, ^{210}Po, and ^{90}Sr. The aim of this study is to facilitate the design of an RTG with a minimal radiation dose rate and mass including any required shielding. Applications of interest are primarily space and planetary exploration. In order to evaluate the properties of the alternative radioisotopes a Monte Carlo model was developed to examine the radiation protection aspect of the study. The thermodynamics of the power generation process is examined and possible materials for the housing and encapsulation of the radioisotopes are proposed. In this study we also present a historical review of radioisotope thermoelectric generators (RTGs) and the thermoelectric conversion mechanism in order to provide a direct comparison with the performance of our proposed alternative isotope systems.

1. Introduction

Radioisotope heating units (RHUs) and radioisotope thermoelectric generators (RTGs) have been successfully employed on a number of space missions and extensively used in terrestrial applications. Russian built 'Beta-M' RTGs fuelled with Strontium-90 were deployed in unmanned lighthouses, coastal beacons and remote weather and environment monitoring stations and had a typical power output of around 230 Watts electrical (W_e) [1]. The original network of automatic weather stations (AWSs) in Antarctica was powered by RTGs; however, by the early 1990s safety concerns led to the removal of these power sources [2]. Today, RTG devices have become safer in design due to advances in material fabrication techniques.

Efficient power production has always been one of the challenges of the exploration of space and the solar system. The challenge is even greater at increasing distance from the Sun or beneath planetary surfaces, where solar light intensity levels and extreme temperatures could preclude the use of solar power and chemical power generation systems. Additional power burdens on the budgets available for certain missions may be imposed by systems that have specific operating temperatures and temperature control requirements. Radioisotope power sources are capable of providing both thermal control and electrical power. Reducing the mass and maximising the efficiency of radioisotope power sources will have a positive impact on the overall mass budgets of science payloads and the range of mission scenarios for a specific project.

To date, ^{238}Pu has been the most commonly used RTG and RHU isotope for space applications. Plutonium-238 decays primarily by alpha emission, where the energy of the alpha particle is ~5 MeV. Plutonium-238 can also decay by spontaneous fission with a very low probability [3]. The absorption of the alpha particles (and any fission products) will produce heat that can be exploited to generate electricity by means of a power conversion system, in the form of thermoelectric junctions or other power conversion cycles (see Section 1.3). Current concerns over the limited supply and the cost of producing ^{238}Pu [4] has increased the need to explore alternative isotopes for these applications. The radioisotopes that are presented as a possible solution by this paper are ^{241}Am, ^{208}Po and ^{210}Po. The use of ^{90}Sr is also discussed briefly.

1.1. The US SNAP program

Under the systems nuclear auxiliary power (SNAP) program, a range of RTGs and small reactors were developed in the United States for space and military use. The RTGs developed were successfully flown on several satellite and space exploration missions [5]. The efficiencies of some of the early devices were between 4% and 5% [6]. This was due to limitations in the power conversion process and losses within the system. Latter devices such as the

* Corresponding author. Tel.: +44 1162522902; fax: +44 1162522464.
E-mail address: rco3@star.le.ac.uk (R.C. O'Brien).

0022-3115/$ - see front matter © 2008 Elsevier B.V. All rights reserved.
doi:10.1016/j.jnucmat.2008.04.009

multi hundred watt (MHW) power sources flown on the voyager missions and the general purpose heat source RTGs (GPHS-RTG) as flown on board Galileo and Cassini missions have efficiencies of the order of 6.6% [6].

SNAP-19 devices were successfully used on the Nimbus meteorological satellites [reference], Pioneer 10 and 11 [5] and were also included in the Viking 1 and 2 mars lander missions. The SNAP-19 devices were loaded with $^{238}PuO_2$–Mo fuel cermets with a total activity ranging from 34.4 to 80 kCi [6] depending on the mission and application.

The SNAP-27 devices that were landed on the moon during the Apollo 12, 14, 15, 16 and 17 missions were designed to provided a beginning of life (BOL) output power of 63.5 W_e (electrical power in Watts) and a specific power density of 3.2 W_e /kg [6]. The total activity of the SNAP-27 fuel source was 44.5 kCi and consisted of microspheres of $^{238}PuO_2$ ceramic [6]. These devices had a power conversion system with a 5% efficiency based on PbSnTe junctions. The output voltage of the devices was between 14 and 16 V D.C. SNAP-27 devices were used as power sources for lunar surface science experiments with life spans ranging from 4 to 8 years (Fig. 1).

The failure of the Apollo 13 mission enabled the testing of the integrity of the SNAP-27 design during the re-entry of the lunar module into the Earth's atmosphere. The lunar module splashed down in the Tonga Trench, which is in the Pacific Ocean. No measurements of contamination have been made to date and it is assumed that the SNAP-27 fuel capsule is intact at a depth of 6.5 km below the surface of the ocean.

Even though the integrity of the SNAP design during re-entry is not in question, the additional mass of the aeroshell and cask used by this system reduced the overall system power density which could be improved today by the adoption of alternative encapsulation techniques.

Following the SNAP programmes, the US developed the multi-hundred watt (MHW) RTG systems to provide power to the Lincoln experimental satellites LES 8 and 9 and Voyager 1 and 2 spacecraft. These devices were fuelled by 24 pressed spheres of $^{238}PuO_2$, each with an activity of 3.2 kCi. Each sphere was encapsulated within a cladding of iridium alloy and housed individually within a filament wound carbon–carbon impact shell. All 24 assembled spheres were housed within a cylindrical POCO graphite aeroshell for re-entry protection [6]. The thermoelectric conversion was performed using SiGe junctions [8] with an efficiency of 6.7% [6]. The MHW RTGs had a beginning of mission power level of 2.4 kW_{th} [8] or 160.8 W_e. The overall beginning of mission system power density was 4.2 W/kg [8].

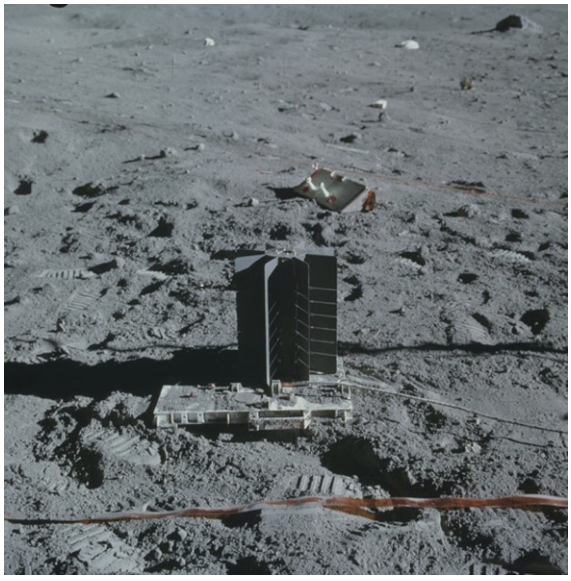

Fig. 1. SNAP-27 RTG deployed on the lunar surface during the Apollo 16 mission [7].

1.2. Current space battery technology

The general-purpose heat source radioisotope thermoelectric generator (GPHS-RTG) is a power source that features an integrated modular heat source design [9] (see Fig. 2). Originally designed for the Galileo spacecraft, the GPHS-RTG was successfully used for the NASA Cassini mission and more recently, the New Horizons Kuiper belt mission. The GPHS-RTG was originally built by the US Department of Energy (DOE) at the Mound Laboratory in Miamisburg, Ohio. As a result of increased security requirements and costs the DOE closed the Mound site. The responsibility for assembling RTGs was transferred to a new space battery facility at the Idaho National Laboratory Materials and Fuels Complex (MFC). This was done prior to the 2006 New Horizons mission.

A general purpose heat source (GPHS) module is a composite carbon body that houses a total of four fuel pellets and as a whole acts as an aero-impact shell. The isotope fuel for the GPHS-RTG is in the form of plutonium dioxide ($^{238}PuO_2$) at approximately 80% density. The fuel is pressed into pellets with an approximate length and diameter of 27.6 mm [9]. Each pellet has approximately 0.55 mm of iridium alloy (DOP-26) cladding [9] that is used to maintain the structural integrity of the pellet both under normal operating conditions and under impact. The iridium cladding also

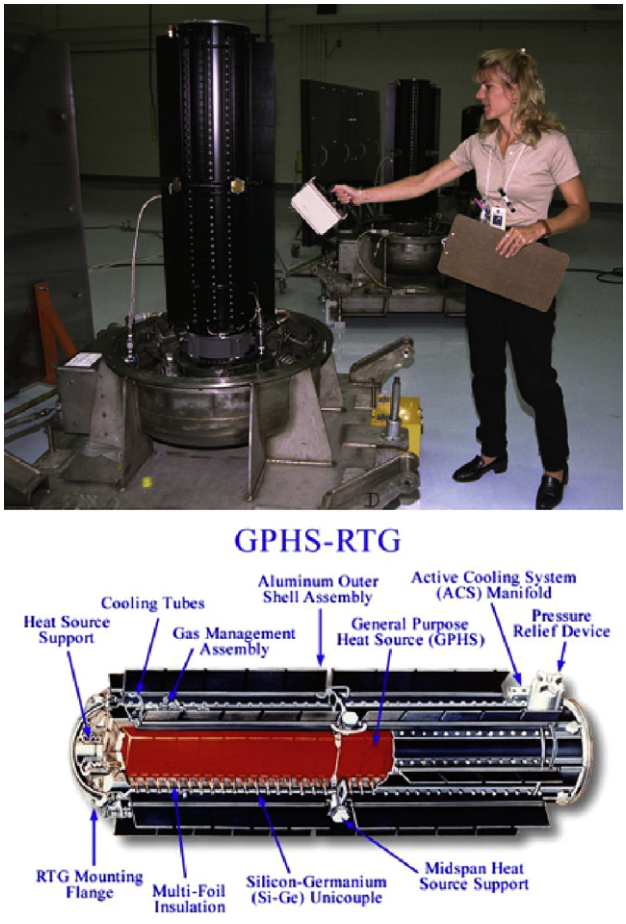

Fig. 2. Top; pre-flight checkout of the Cassini GPHS-RTGs – courtesy NASA/KSC. Bottom; A cutaway schematic of the GPHS RTG – courtesy NASA/JPL-Caltech.

prevents the interaction of the source alpha particles with materials with low atomic masses, which could produce neutrons via α-n reactions. The internal structure of the GPHS module consists of two composite impact shells covered by a carbon-bonded carbon sleeve. Each internal impact shell contains two fuel pellets separated by a floating membrane [9]. The thermal power output of a single fuel pellet is approximately 62.5 W_{th} [9]. GPHS modules can be stacked together and thermally coupled. The required electrical output power levels are achieved through the appropriate selection of a number of GPHS modules incorporated in a RTG system. The number of modules required is directly related to the power conversion efficiency of the system. The current GPHS-RTG systems have a power conversion efficiency of 6.5% to 7% and an overall system power density of 5.2 $W_e\ kg^{-1}$ [6] if a stack of 18 GPHS modules is used [9]. The thermoelectric junctions used for power conversion by the GPHS-RTG are SiGe type junctions.

The ^{238}Pu fuel that is used within the GPHS-RTG systems is currently supplied to the US Department of Energy (DOE) by Russia in the form of $^{238}PuO_2$ powder with an activity of between 12.6 and 15.1 Ci g^{-1}. The radioisotope is manufactured by the proton irradiation of ^{237}Np or via the neutron irradiation of ^{237}Np in a high flux reactor. The latter is the more commonly used method and results in the production of ^{238}Np (half-life of 2.117 days), which decays via beta emission into ^{238}Pu. Current concerns over the supply of ^{238}Pu [4] have prompted the DOE to investigate the feasibility of establishing a production line in the US in order to meet the future needs of NASA [10].

1.3. Power conversion

RTG systems employ thermoelectric power generators, which produce an electric potential by exploiting the Seebeck effect. The Seebeck effect is observed when a temperature gradient exists across the junction of two different metals or semiconductors [10]. The magnitude of the thermoelectric electro-motive force (EMF) across each junction is typically of the order of μV to several mV and is dependant upon junction material selection. An estimate for each junction potential with hot and cold side temperatures (T_H and T_c respectively) can be made using Eq. (1). The Seebeck coefficient α_{pn} can be defined as the thermoelectric voltage generated across a junction of thermoelectric materials p and n subjected to a junction temperature difference ($T_H - T_C$) and is usually stated in units of $\mu V\ ^\circ C^{-1}$. For a junction of SiGe, this has been measured to be on average 135.4 $\mu V\ ^\circ C^{-1}$ [11].

$$V_{\text{junction}} = \int_{T_C}^{T_H} \alpha_{p-n} \cdot dT. \tag{1}$$

Eq. (1) Seebeck voltage for a thermoelectric junction p–n with Seebeck coefficient α_{p-n}.

Multiple junctions are electrically connected in series to provide the required power. Thermoelectric generator module junctions are typically assembled such that the cold side of the semiconductor element is soldered to a metal cap and the hot side connection is made by compressively loading the element against the hot junction connecting-shoe. Multiple structures can be assembled in the same way [12]. This method of assembly leads to the requirement for the modules to be installed within the RTG system under mechanical compression [12].

RTG systems can exploit conduction, convection or radiative processes to transfer heat to the conversion units. Certain systems may utilise a combination of these methods. One of the main advantages of using radiative transfer in place of conduction or convection is the uniformity of the temperature of the hot junction [12]. The fundamental disadvantage of heat transfer via thermal radiation is the high temperature requirements placed on the heat source. High operating temperature requirements have a direct influence on the materials used within the system and hence the overall system mass.

Alternative power conversion technologies are currently being studied, including: thermionic [13], thermophotovoltaic [14], Brayton and Stirling power conversion systems [15]. The use of Stirling electric generators has recently been of great interest to several research institutes including the NASA Glenn Research Center, Cleveland, Ohio [16]. The main interest behind this research lies with the desire to improve on the power conversion efficiency of current thermoelectric based radioisotope power sources [17], which today have efficiencies of the order of 6.5–7% [6]. The power conversion efficiencies of modern Stirling generators is placed between 22% and 32% [16].

Despite their greater conversion efficiencies, mechanical systems such as Stirling generators have a much greater mass than thermoelectric systems. It is suggested that the greater efficiency allows for a reduction in fuel mass when compared to current GPHS-RTG systems [18]. However, this fuel saving is unlikely to translate into a net system mass saving. Concerns over the operational lifetimes of mechanical systems operating in a high radiation environment and the need to the balance the mass associated with such a unit is addressed by having a dual-device deployment strategy. This strategy has called into question the economics of mechanical power conversion. For these reasons, more research into the overall benefits of using these systems in place of the thermoelectric based systems is required. Research into alternative solid-state power converters and hybrids of these technologies will prove to be vital to the improvement of conversion efficiency and the minimisation of system mass.

2. Reduced neutron and gamma ray radiation emissions

The careful selection and design of the radioisotope fuel source will make it possible to derive the most mass efficient shielding configuration. The selection of an isotope for a specific application is dependent on several requirements. These requirements include; mission duration, electrical power levels, whether the device is to be used for heating in addition to the generation of electricity, proximity to sensitive instrumentation and biological systems, and the overall mission mass budget.

A range of isotopes were considered throughout this section of our study as potential candidates to replace ^{238}Pu in RTGs. These included ^{241}Am, ^{210}Po, ^{208}Po and the already extensively used ^{90}Sr. These isotopes are primarily alpha particle sources with the exception of ^{90}Sr, which undergoes beta decay.

Despite its high thermal power density (see Table 1), the use of ^{90}Sr as a direct substitute for ^{238}Pu in the GPHS architecture and use within a low mass heat source is impractical without enhancement of shielding structures due to the emission of secondary gamma rays; 2 MeV gamma rays from ^{90}Y [19], the short-lived daughter nuclei from the beta decay of ^{90}Sr.

A similar problem is exhibited by the use of ^{243}Cm, which has an alpha particle energy spectrum that includes alpha energies of 6.0, 5.8 and 5.7 MeV with relative emission probabilities of 6%, 81% and 13%, respectively [20]. Although the isotope has a high power density, it also has a total Gamma Ray emission probability of 61.6% per decay with an average energy of 130 keV [21]. Simple shielding with high density materials would be able to dramatically reduce the flux of low energy Gamma Rays with a mass penalty.

^{210}Po has been considered and demonstrated historically as an alpha source for fuelling RTGs [22]. ^{210}Po has a specific activity of 4.5 kCi g^{-1} and a power density of 137 $W_{th}\ g^{-1}$. The half-life of ^{210}Po is 138.38 days [19]. When compared to ^{238}Pu under the SNAP program, the shorter half-life of ^{210}Po resulted in the favoured use

Table 1
Summary of the key properties of the isotopes presented

Isotope and form	Decay	Half life (years)	Theoretical specific activity (Ci g^{-1})	Theoretical specific thermal power (W g^{-1})	Density (g cm^{-3})	Neutron flux (n s^{-1} g^{-1})	Average charged particle energy (MeV)	Gamma ray energy (keV)	Mass required for 5 W_e (g)
^{238}Pu	α	87.74	17.13	0.557	19.84	2.932×10^3	5.49	43	180[a]
	γ							99	
Pure isotope	Spont. fission							152	
^{238}Pu	α	87.74	15.10	0.491 [0.345[b]]	11.46	3.030×10^4 (natural oxide)	5.49	43	200[a]
	γ							99	
PuO_2 aged 30 years	Spont. fission					2.697×10^3 (enriched oxide)		152	
^{241}Am	α	432.70	3.43	0.111	13.67	1.364	5.46	26	900[a]
	γ							33	
Pure isotope	Spont. fission							59	
^{241}Am	α	432.70	2.73	0.089	11.68	5.321×10^3 (natural oxide)	5.46	26	1124[a]
	γ							33	
AmO_2	Spont. fission					1.080×10^2 (enriched oxide)		59	
^{208}Po	α	2.898	590	17.81	9.30	–	5.12	[c]	6[a]
Metallic	γ[a]							None	
^{210}Po	α	0.38	4493	137	9.30	–	5.30	[c]	0.7[a]
Metallic	γ[a]							None	
^{90}Sr	β	28.78	110.38	0.128	5.10	–	0.546 (2.28 from ^{90}Yr)	2000 (^{90}Yr)	781[a]
SrO									

[a] Based on a 5% conversion efficiency.
[b] Calculated from data presented by Bennett et al. [5] for current materials (approx. 25–30 years old).
[c] Very low probability of emission.

of ^{238}Pu for space applications. The delay between generator assembly and launch required a much greater beginning of life power in order to deliver the minimum beginning of mission power levels associated with ^{238}Pu fuelled power sources.

Both isotopes of Polonium have a single step alpha decay chain resulting in the formation of stable ^{206}Pb and ^{204}Pb, respectively. Less than 1×10^{-3}% of the decays of ^{210}Po and ^{208}Po result in gamma ray production with respective energies of 803.1 keV and 291.8 keV. ^{210}Po and ^{208}Po have a respective specific power density of 400 and 52 times that of ^{238}Pu. Given the negligible gamma ray emission rate from these sources, very little high density shielding is required for systems fuelled with the Po isotopes. Both isotopes of polonium have a very low melting point (252 °C) and a boiling point of 962 °C [23]. For this reason careful consideration must be made into heat rejection systems for the pure isotope so as to prevent its vaporisation.

^{208}Po is produced commercially by means of proton irradiation of ^{207}Bi targets inside a cyclotron. ^{210}Po is most cost effectively produced by neutron irradiation of ^{209}Bi inside a nuclear reactor. The capture of neutrons by ^{209}Bi nuclei results in the production of ^{210}Bi which has a 5 day half-life [19] and decays by Beta emission to ^{210}Po.

Despite the requirement for large beginning of life power levels, the use of ^{210}Po and ^{208}Po as RTG power sources could be considered for deep space missions provided that an adaptive heat exchange system could be used to maintain an appropriate temperature gradient across the power conversion system. Such a system may feature a pumped cooling fluid such as liquid metals. Adjustment of the flow rate of working fluid would allow for tuning of the heat flow from the cold side of a power conversion system to a heat rejection mechanism. Such mechanisms would result in a mass penalty and could effectively lower the system power. This would also add to the complexity of the system and may call for the qualification of the operational life-time of the system. For this reason when considering the, the isotopes of Polonium are better suited to short duration mission applications due to their short half lives (2.898 and 0.38 years for ^{208}Po and ^{210}Po respectively [19]).

Americium-241 has a specific thermal power that is approximately one fifth that of ^{238}Pu and a half-life that is approximately five times greater than that of ^{238}Pu. The spontaneous fission probability for ^{241}Am is 4.30×10^{-10}% of all decays. This is equivalent to a 10^3 reduction in neutron flux when compared to an equivalent amount of ^{238}Pu in their pure isotopic form. The maximum photon energy produced by ^{241}Am is 59.5 keV [19]. These photons can easily be shielded using relatively thin layers of high density materials. Three millimetres of aluminium shielding would reduce the intensity of the gamma ray radiation to 1% of its original. In addition to this, ^{241}Am is also easily extracted from stockpiles of transuranic waste; the bi-product of nuclear fission reactors. The production of ^{241}Am occurs in two steps. Firstly ^{241}Pu is formed during double neutron capture reactions within the core of a reactor. ^{241}Pu has a half-life of 14.4 years and decays via beta emission to form ^{241}Am [19]. Figs. 3 and 4 illustrate the spontaneous fission neutron spectra that dominate for pure ^{241}Am and ^{238}Pu sources. The data illustrated in Figs. 3 and 4 was produced through the modelling of a 1 cm^3 source consisting of the corresponding isotopes using the Monte Carlo N-Particle transport code MCNPX 6^{TM} [24]. Using this code, the source was assigned appropriate spontaneous fission probabilities (1.85×10^{-7}% of decay events for PuO_2 [3] and 4.30×10^{-10}% of decay events for AmO_2 [3]) and a neutron energy spectrum was calculated by means of a tally function throughout the volume of the source. The statistics generated by these MCNPX simulations were resultant from the calculation of $1x10^6$ spontaneous fission events.

Both ^{241}Am and ^{238}Pu are chemically stable under the operating temperatures and conditions (<1000 °C) in their oxide forms. These are AmO_2 and PuO_2 respectively. These oxide compounds are formed when Americium nitrate or Plutonium nitrate is heated in an oxygenated atmosphere (air) between 700 and 800 °C. Natural oxygen is composed of 99.757% ^{16}O, 0.038% ^{17}O and 0.205% ^{18}O [19]. The threshold energy for the ^{16}O alpha-neutron (α,n) reaction is 15.24 MeV [25] and hence this particular reaction does not occur for ^{238}Pu or ^{241}Am in their oxide compounds. Although low in concentration, the (α,n) reaction cross-sections for ^{17}O and ^{18}O are significant for alpha particles with energies in the range from 0 to 6 MeV. Quantitatively, for alpha particles with energies of 5.5 MeV, the cross-sections of ^{17}O and ^{18}O are 206 milibarns and 440 milibarns respectively [26]. The ^{17}O (α,n) reaction has a Q value of +0.587 MeV and a threshold energy of 0 MeV [27]. The

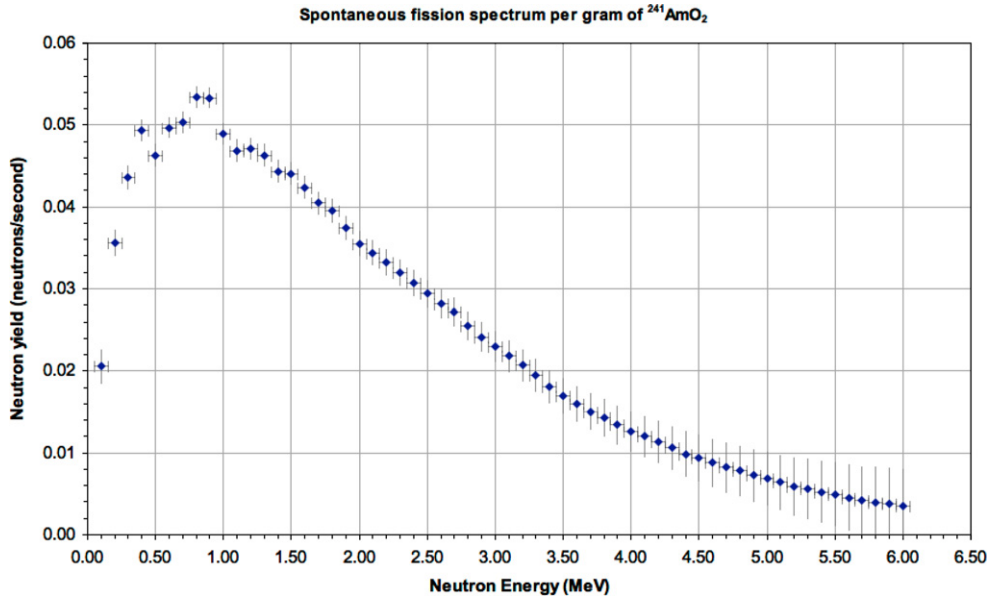

Fig. 3. Spontaneous fission (S.F.) neutron yield per gram of ^{241}Am. This S.F. spectrum was generated using the Monte Carlo N-Particle transport code MCNPX version 6 [24], the statistics from which were derived from the calculation of 1×10^6 spontaneous fission events.

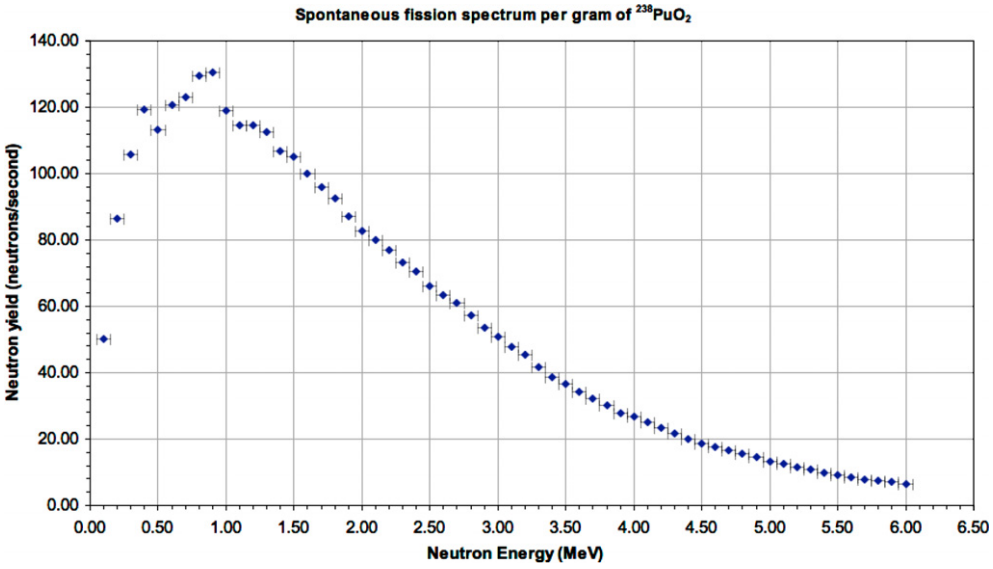

Fig. 4. Spontaneous fission (S.F.) neutron yield per gram of ^{238}Pu. This S.F. spectrum was generated using the Monte Carlo N-Particle transport code MCNPX version 6 [24], the statistics from which were derived from the calculation of 1×10^6 spontaneous fission events.

^{18}O (α,n) reaction has a Q value of -0.697 MeV and a threshold energy of 0.852 MeV [27]. Thus, for pure isotopes with predominantly low spontaneous fission probabilities, and hence relatively low neutron flux, when an oxide or dioxide compound of such isotopes is formed, an entirely different neutron emission spectrum is produced.

In order to facilitate accurate modelling of RTG radiation sources, the calculation of a total neutron energy spectrum was necessary. By treating the radiation source as a homogenous mixture of oxygen and the parent radionuclide with a unified molar mass M_0, it is possible to estimate the stopping power of the matrix [28]:

$$\frac{dE}{dx} = \left(\frac{e^2}{4\pi\varepsilon_0}\right)^2 \left(\frac{N_A\rho}{M_0}\right)\left(\frac{4\pi z^2 Z}{mc^2\beta^2}\right)\left[\ln\left(\frac{2mc^2\beta^2}{10Z}\right) - \ln(1-\beta^2) - \beta^2\right]. \quad (2)$$

Eq. (2): The Bethe Bloch formula for a material with molar mass M_0, density ρ and reaction target atomic number Z for an incident particle with charge z and velocity v (where β is the ratio of velocity to speed of light c) [28,29].

Using the stopping power of the compound matrix it is possible to estimate the neutron yield for a thick source. An energy spectrum can easily be obtained from Eq. (2)

$$Y = I\left(\frac{N_A\rho}{M_0}\right)\int_{E_0}^{E}\sigma(E)\frac{dx}{dE}\cdot dE. \quad (3)$$

Eq. (3) Neutron yield for a thick target of compound with molar mass M_0 and density ρ where σ is the reaction cross section as a function of energy [29,30].

Total neutron spectra were produced for both AmO_2 and PuO_2 by the combination of their spontaneous fission neutron spectra

and the neutron yields as a result of (α,n) -reactions with ^{17}O and ^{18}O obtained through the application of Eqs. (2) and (3). These spectra are illustrated in Figs. 5 and 6.

It can be deduced from Figs. 5 and 6 that the neutron yield from the (α,n) reaction with ^{17}O and ^{18}O is the dominant feature in the total neutron spectra for both $^{238}PuO_2$ and $^{241}AmO_2$. Upon examination of the total neutron yield per gram of ^{241}Am and $^{241}AmO_2$, there is a stark contrast. The neutron yield for ^{241}Am in a pure metallic form is around 1.353 n s^{-1} g^{-1} (derived from spontaneous fission), whereas that of AmO_2 is around 5.321×10^3 n s^{-1} g^{-1}. For metallic ^{238}Pu the neutron yield is around 2.932×10^3 n s^{-1} g^{-1} and for PuO_2 the neutron yield is of the order of 3.030×10^4 n. s^{-1} g^{-1}. These results and the spectra illustrated in Figs. 5 and 6 were verified using the SOURCES 4C code [31].

If a reduction in the total neutron yields for both AmO_2 and PuO_2 is required for safety, chemical processing of the materials may be performed which includes oxygen enrichment. The principal of oxygen enrichment is to alter the composition of the oxide from the natural oxygen isotopic ratios to one that is mostly composed of ^{16}O. A process has been established for the oxygen enrichment of $^{238}PuO_2$ [32]. This process involves the heating of PuO_2 formed in a natural oxygen environment up to around 1000 °C while simultaneously subjecting the materials under positive pressure to a flow of ^{16}O enriched oxygen carried in Argon gas [33] with approximately 4:1 flow ratio of ^{16}O to argon [32]. This main procedure is undertaken for approximately 30 min and allows the ^{16}O atoms to exchange from the gas flow into the PuO_2 ceramic while the exhaust flow from the process carries away approximately 98% of the original ^{17}O and ^{18}O content. The processing time is the main driving variable for the final level of enrichment for any given ^{16}O flow rate and processing temperature. The resultant reduction in the neutron flux for oxygen-enriched PuO_2 is approximately

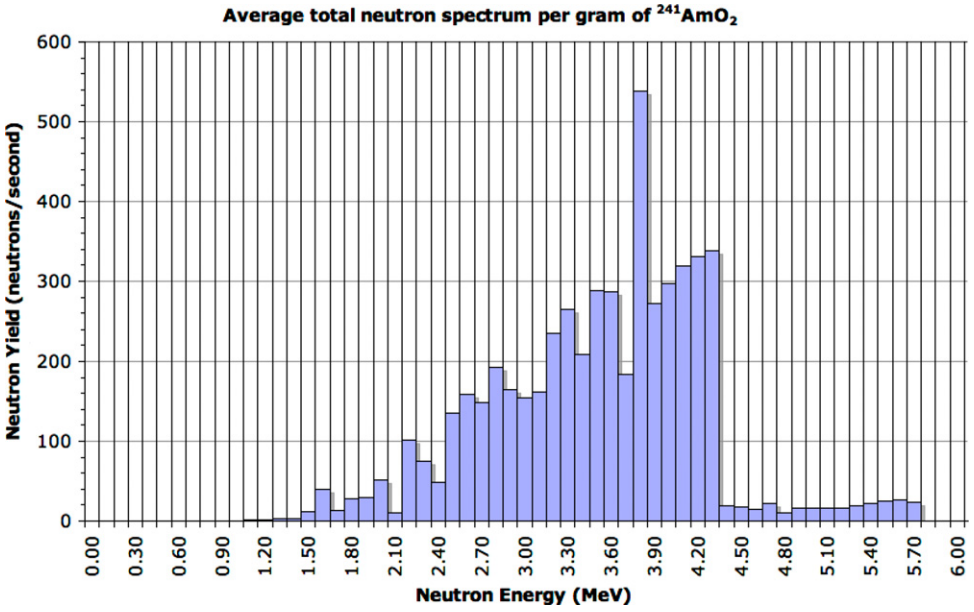

Fig. 5. Total neutron yield per gram of $^{241}AmO_2$ compound matrix based on an average α energy of 5.46 MeV.

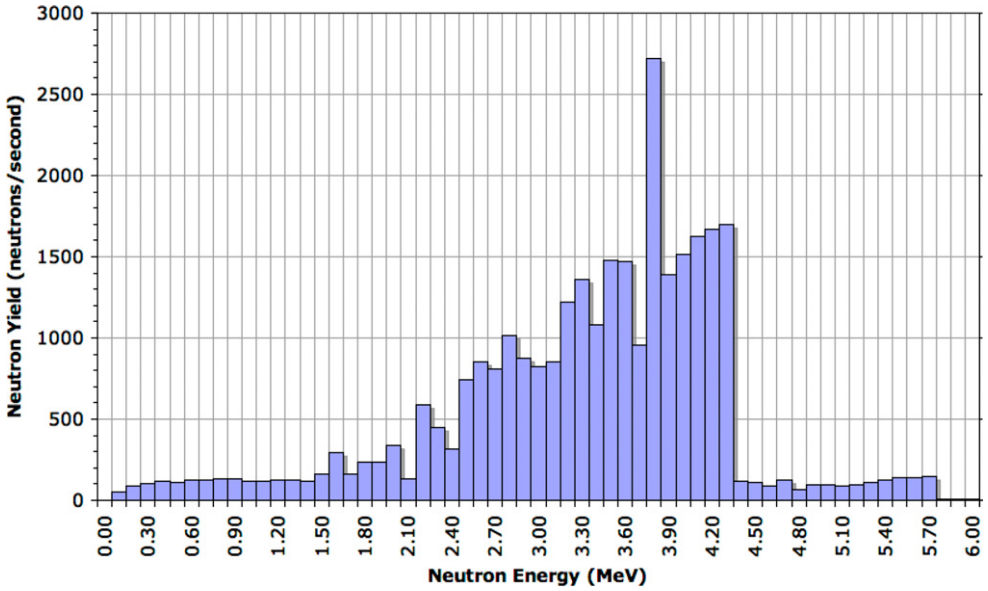

Fig. 6. Total neutron yield per gram of $^{238}PuO_2$ compound matrix based on an average α energy of 5.49 MeV.

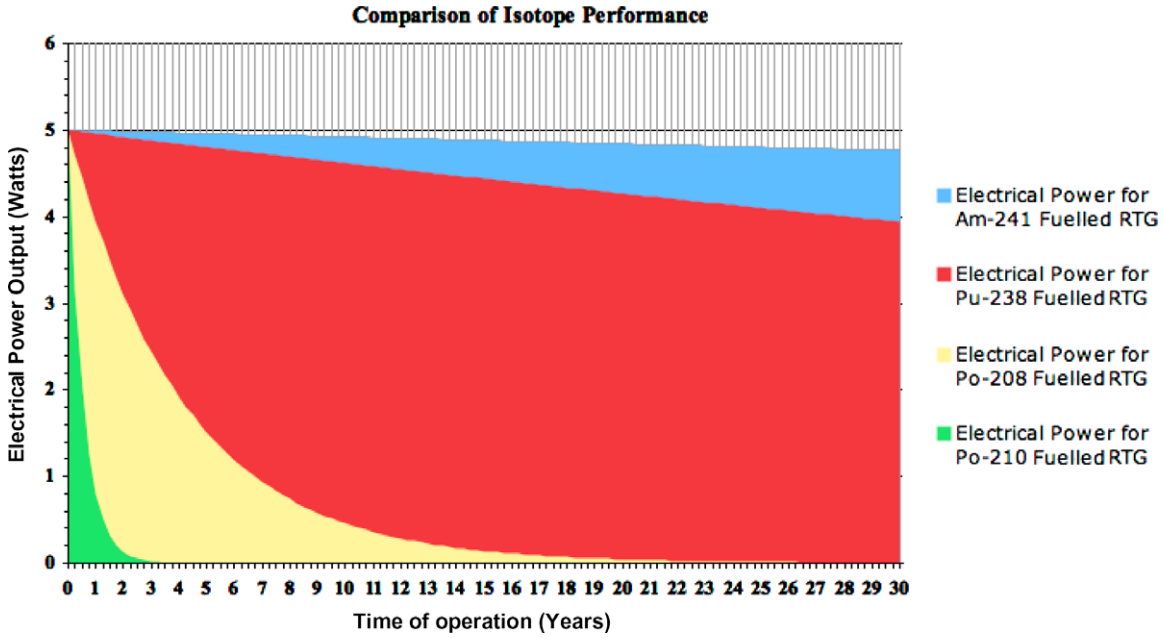

Fig. 7. A plot of calculated system performances for theoretical RTGs with a beginning of mission power output of 5 W_e fuelled by candidate alternative reduced radiation isotopes. These performances are compared to that of a similar device fuelled by ^{238}Pu.

91.1% [32] down to around 2.697×10^3 n s^{-1} g^{-1}. In terms of the yield due to a–n reactions, oxygen enrichment reduces the α–n neutron yield from 92% of the total flux to a contribution of only 13.4% of the total yield (approx. 359 n s^{-1} g^{-1} of $^{238}PuO_2$). Thus, approximately 86.6% of the total neutron yield for oxygen-enriched $^{238}PuO_2$ is derived from spontaneous fission.

Given the level of success of the oxygen enrichment processing of PuO_2, it is equally conceivable that an almost identical process can be applied to the enrichment of AmO_2 materials. Under such processing, the maximum permissible exchange temperature should not exceed 1100 °C, the dissociation temperature of AmO_2. Assuming that the oxygen exchange process can achieve the same degree of ^{16}O purity and given that ^{241}Am produces 10^3 times fewer spontaneous fission neutrons than ^{238}Pu, it is estimated a 97.97% reduction in the total neutron yield for $^{241}AmO_2$ can be achieved. This would result in a total neutron yield of approximately 1.08×10^2 n s^{-1} g^{-1} of $^{241}AmO_2$.

The radioactivity properties for the isotopes determined above is summarised in Table 1. Table 1 also includes basic material properties for each isotope along with common physical forms.

In order to assist in the selection of the most appropriate isotopes for use under a space or planetary mission architecture, a plot of electrical power output versus mission time was generated for a typical beginning of mission power level for a modern surface experiment. See Fig. 7. The beginning of mission power level chosen for this study was 5 W_e since this is also typical of the order of what would be required to provide power for an electric propulsion system that may augment or provide alternative/redundant propulsion for an outer planet or Kuiper belt space mission. As can be seen in Fig. 7, after 30 years of operation, ^{241}Am fuelled sources are capable of delivering approximately 95.3% of the beginning of mission power. After the same period, ^{238}Pu fuelled devices can deliver a maximum of 78.9% of the beginning of mission electrical power.

As expected, the results in Fig. 7 show that ^{210}Po and ^{208}Po sources are ideal for missions where the thermal power and radioactivity are required to drop to a minimum after a relatively short operating period. Both isotopes decay into stable lead. An example of such requirements may be for use by probes that are required to penetrate through ice sheets on icy moons or for terrestrial glaciology studies. Once the required depth has been achieved, the thermal output of the system would decay to a negligible level after a relatively short period and would have little impact on the environment.

3. Radioisotope fuel cermets and encapsulation

Fuel cermets have been examined as a means of encasing fissile fuels for use in reactor systems such as in nuclear thermal rocket propulsion [34]. Cermet (ceramic–metallic) encapsulation is the formation of a material matrix composed of an intimate mixture of metallic carrier material and a ceramic compound such as a radioisotope in its oxide form. A cermet matrix may alternatively be formed where the ceramic materials are used as a carrier material for a metallic material. The matrix density can be tuned as desired so as to control the overall strength and porosity of the structure in addition to the control of migration of the contained materials. This technology can be applied to the carriage of isotopic materials within a stable and secure metallic carrier. The Transit-RTG and the SNAP-19 RTG both used a plutonium dioxide–molybdenum fuel cermet that was encapsulated in refractory metal cladding for containment [6]. During the ROVER/NERVA nuclear thermal rocket programs, uranium fuel was dispersed into a graphite matrix [35]. This had the disadvantage of being chemically unstable in a high temperature hydrogen environment [36], which led to the structural failure of the reactor cores and release of fission products into the exhaust stream. Current research into tungsten matrix cermets is expected to overcome the problem of the high temperature stability. Tungsten exhibits good thermal conductivity and has a high melting point. In addition to this, it has been demonstrated that a tungsten matrix is capable of containing any gaseous fission products up to a temperature of 1550 °C [37]. Although the density of tungsten is much greater than that of graphite, the physical properties of the material result in a much smaller volume requirement.

The high melting point of tungsten may be sufficient to prevent the release of encapsulated radiological materials during an

accidental re-entry, launch failure or re-entry anomaly associated with any space mission. This should be validated through computational modelling and experimental testing. The encapsulation of the radioactive materials in tungsten could provide additional radiation shielding. The effect of the encapsulation in tungsten on the radiation dose, for various isotopes, has been evaluated by Monte Carlo methods (see Sections 4 and 5).

Traditional fabrication of the fuelled cermets is undertaken at both high temperatures and high pressures using an isostatic sintering process. Sintering of pre-pressed matrices requires the materials to be heated up to temperatures above their melting temperatures for a prolonged period [38]. The combination of high temperature with isostatic pressing in a single process (known as hot isostatic pressing or 'hipping') ensures uniform consolidation of materials at temperatures below their melting points. Spark plasma sintering (SPS) is a relatively new powder metallurgy technique that is capable of greatly reducing the average sintering temperature [38] and minimising grain growth that is typically observed using the traditional sintering techniques [39]. In the SPS process, a powder mixture is heated by Joule heating which is a result of the passing of electric current through the powder matrix that is to be consolidated. This is effectively the same as conventional resistive heating with the exception that the temperature is varied throughout the process by the pulsation of the current. There are therefore two distinct operating temperatures for an SPS furnace; the average temperature, and a much higher temperature that is only reached during the flow of the current pulses. The average temperature is tuned to be lower than the melting point of the materials in the matrix. This therefore reduces or prevents the dissociation of the molecules of the encapsulated materials.

The overall setup consists of a conductive (graphite) die into which the powder mixture is formed, a press and a high power pulsed DC circuit. The die, and ultimately, the powder mixture itself form the completing component for the DC circuit. The geometry of the die determines the radial geometry of the pressed/sintered cermet. The powdered fuel (in oxide form) and tungsten metal powders, typically less than 10 μm in grain size, are mixed to the desired ratio. Once prepared, the mixture is loaded into the graphite die. The die is then put under compression in between two electrodes in a hydraulic press [40] in order to compact the mixture. At this point a current is passed with a discharge pulse of the order of several tens of kA, and its duration is of the order of several hundreds of microseconds [41].

During each current discharge, metallic material is transported by the spark propagation across the pores of the matrix. When the current is switched off, the matrix undergoes rapid cooling resulting in the condensation of the metallic vapours within the regions where there is mechanical contact between powder grains [41]. This condensation of vapour produces necks that enhance these joints. The material transport in subsequent spark pulses is accentuated due to the greater electric current density in the necks and contacts than inside the body of each powder grain. The rate of material transport is enhanced through the application of an external compressive force [43] resulting in the plastic deformation of the powder grains at each interface [39] resulting in a flatter joint with lower electrical resistance. This process propagates throughout the matrix enhanced by the external pressure which induces plastic flow of the material to form a sintered cermet with a density that is very close the full theoretical density. This process propagation is similar to that exhibited in the consolidation of matrices by hot isostatic pressing [39]. This process is illustrated in Fig. 8.

For isotopic fuels that produce heat through alpha decay, it is important to consider the probability of (α,n) reactions contributing to the radiation flux or dose generated by the source. This effect should be minimised during the matrix design process by calculated materials selection. Generally, materials with high atomic numbers will reduce the contribution from (α,n) reactions. Thus tungsten is again a favourable material for cermet fabrication. Using the SOURCES 4C code [31] it was estimated that a 57% reduction in the (α,n) reaction derived neutron flux can be achieved by producing an intimately mixed matrix composed of 50% $^{241}AmO_2$ and 50% Tungsten by volume. This neutron flux can be reduced by a total of 65.9% by changing the volumetric composition of the matrix to 40% Tungsten. It is believed that a cermet consisting of 50% $^{241}AmO_2$ by volume is approximately the maximum volume fraction that the fuel material can occupy without affecting the matrix integrity and strength. This will be evaluated in future work.

In order to minimise thermal stresses across a fuel cermet, the geometry must be designed so as to minimise the temperature gradient across the cermet radius. Finite element modelling (FEM) and

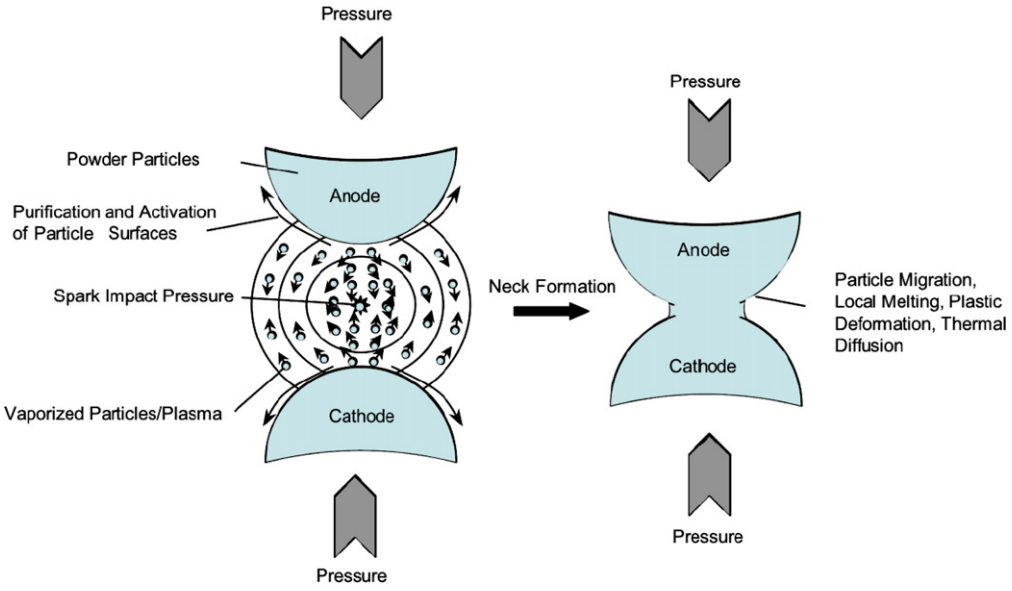

Fig. 8. Spark plasma sintering (SPS) principal schematic showing the consolidation of powdered material through neck formation and applied pressure [42].

analysis of the cermet thermal environment is used to minimise the radial temperature gradient while maximising heat transfer to a thermoelectric conversion system. In the development phase of the project we aim to develop a generic prototype tungsten cermet. Varying amounts of fuel simulant will be added to test the thermal mechanical and chemical properties of the structure.

The alpha decay process within a tungsten-isotope cermet will result in the production of helium nuclei. This helium production could be detrimental to the integrity of the cermet structure given that, for example, per kilogram of plutonium there are approximately 0.3 μmol of helium produced per day. In order to prevent helium cavity formation within the cermet, porosity of the material must be tuned such that helium can be vented. The tuning of cermet porosity occurs during the pressing and sintering processes in such a way that un-pressed cermets will have the maximum porosity and when pressed to maximum density, the porosity is minimised. Experimental results will be used to verify this porosity tuning technique.

The $^{241}AmO_2$–W fuel cermet will be surrounded by a hermetically sealed outer shell or jacket of tungsten or tungsten carbide. Tungsten carbide would ultimately increase the surface hardness, while providing some radiation shielding. This composite structure will reduce the encapsulated cermet mass by up to 19% when compared to a matrix of similar geometry, composed entirely of $^{241}AmO_2$–W. Experimentation into production techniques will be used to verify the effectiveness of this technology. For non-proliferation protection, tungsten carbide can provide resistance against the cutting of the materials while the matrix itself makes extraction of the isotopic materials extremely challenging.

Fig. 9 is a schematic diagram of the geometry described above. The hexagonal tungsten carbide outer shell provides both total encapsulation for the fuel loaded cermet and a mechanical interface for thermo-electric generator (TEG) modules. Each hexagonal face will have two TEG modules, where each module has a footprint of 30 mm × 30 mm.

A similar geometry and encapsulation process using SPS is proposed for isotopes that are typically produced in metallic form such as those of Polonium. Here, an all-metallic matrix could be produced such as Po–W for high strength and high temperature operation, or Po–Al for low mass systems. Again, it may be advantages to include an outer encapsulation shell of tungsten carbide for such matrices for structural integrity and security.

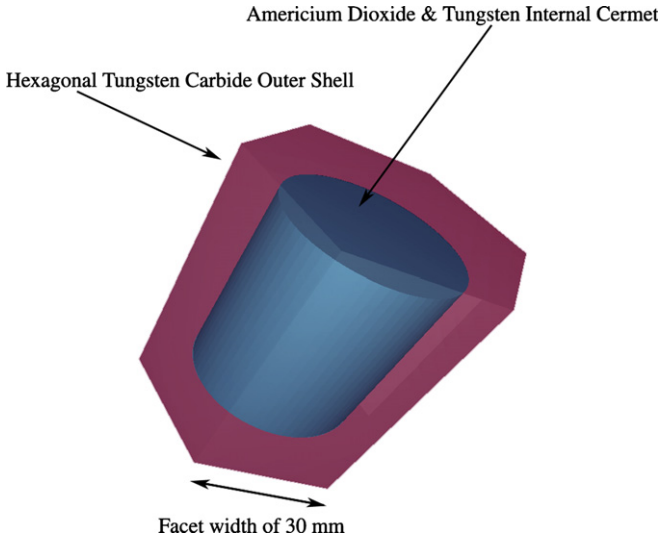

Fig. 9. Prototype hexagonal encapsulated cermet geometry. A tungsten carbide outer jacket surrounds a central americium dioxide/tungsten cermet. The outer jacket has a hexagonal exterior geometry with facet widths of 30 mm so as to facilitate direct coupling with thermoelectric modules.

4. System radiation environment modelling and shielding criteria

Our initial study investigated the theoretical substitution of the GPHS ^{238}Pu fuel pellets with the candidate isotopes listed in Section 5. The study explored the effect of isotope selection on the system mass, thermal power output and radiation dose. The candidate isotopes studied were ^{241}Am in a $^{241}AmO_2$ ceramic pellet form, $^{241}AmO_2$ in tungsten matrices with varying tungsten volume fractions and ^{90}Sr in a ^{90}SrO ceramic form. The study also investigated the effects upon radiation dose by the use of fuels in both natural oxide composition, and in ^{16}O enriched oxide form.

The substitution for ^{238}Pu for polonium was examined with both ^{208}Po and ^{210}Po encapsulated in a tungsten matrix by means of spark plasma sintering (SPS). For the purposes of this study, a 10% pellet volume fraction of polonium was assumed. This encapsulation architecture could maintain capture of all 15.25 g of the polonium loading in each pellet. The hazards associated with this particular substitution are most certainly not attributed to normal operation. Given that polonium has a vaporisation temperature that is lower than the predicted SPS sintering temperature of Tungsten (~1500 °C), production of a consolidated polonium–tungsten matrix may be challenging. Alternatively a polonium–aluminium substitute matrix could be produced since aluminium has been consolidated using an SPS furnace at around 500–550 °C by Zadra et al. [44] given that this is less than the vaporisation temperature of polonium. Such a consolidation would depend upon the existing GPHS module internal aeroshell to ensure safe re-entry of the cermet into the atmosphere but is likely to be able to maintain capture of the polonium loading.

A Monte Carlo model of the GPHS module was created in order to evaluate the effect of isotope selection on radiation dose. The Monte Carlo code MCNPX™ [24] was used to carry out the simulations. The initial model was set up to represent the current GPHS architecture which includes a graphite module casing and two graphite internal aeroshell structures, each containing two iridium clad $^{238}PuO_2$ fuel pellets separated by a graphite floating membrane. In this model, the fuel pellets have an equal length and diameter of 27.6 mm [9] and the iridium cladding has a thickness of 0.5 mm. The activity of each pellet was calculated to be approximately 2.8 kCi based on a specific activity of 15.1 Ci g^{-1} for the $^{238}PuO_2$ ceramic. The output power of each $^{238}PuO_2$ pellet was also found to be 62.5 W_{th}. Graphite was used as a substitute for the

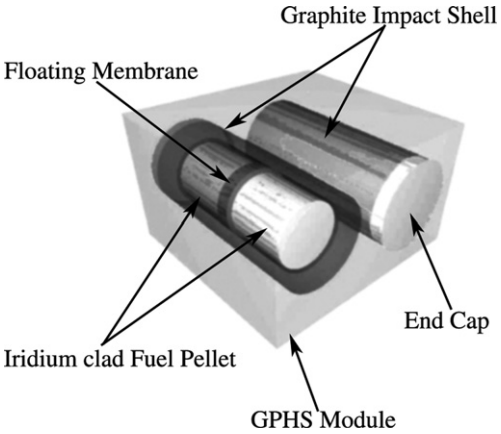

Fig. 10. Three-dimensional drawing of the GPHS module MCNPX [24] geometry model.

carbon-bonded-carbon sleeve that covers the internal aeroshell of the GPHS module. The GPHS geometry model used under the MCNPX software package is illustrated in Fig. 10. The dose rates recorded were calculated for a spherical shell of water with a thickness of 10 mm and an internal radius of 1 m from the centre of the GPHS module.

The results from this study are shown in Table 2. The fuel mass and thermal power output for a single module is represented graphically in Figs. 11 and 12 below. As can be seen in these results, there is a very small mass increase associated with the direct substitution of the original ^{238}Pu plutonium dioxide fuel pellets with ^{241}Am americium dioxide. In addition, there is approximately an 80% reduction in the thermal power output of a single GPHS module.

An advantage of using $^{241}AmO_2$ as a replacement fuel is in the 90% gamma ray dose reduction. For the GPHS architecture, it is clear from Table 2 that encapsulation in a tungsten cermet has an overall detrimental effect on the module mass and thermal power density. Given that the graphite impact shells of the GPHS modules provide protection during critical mission failures such as launch abort scenarios, and that the iridium cladding around the fuel pellets provides some degree of soft X-ray and gamma ray shielding, there is little advantage in using tungsten based matrices for the encapsulation of the AmO_2 fuel as a direct replacement for the current GPHS $^{238}PuO_2$ fuel pellets. However, for non-proliferation safety measures, encapsulation within a tungsten or tungsten carbide matrix may prove to be advantageous.

The application of ^{208}Po and ^{210}Po encapsulated in aluminium matrices to the GPHS architecture is extremely attractive for small systems that demand a high initial power density over relatively short durations. As discussed in Section 2, the mission duration and minimum power requirements would ultimately define the suitability of such isotope selection. It is appreciable that for future lunar missions, small dynamic converter based isotope power systems that take advantage of the GPHS architecture by using 1 or 2 GPHS modules, such as the NASA advanced stirling radioisotope generator (ASRG), could be a potential application for the ^{208}Po isotope. Under such an application, it is quite conceivable that a system similar to the ASRG could provide up to 580 W_e for a minimum of 2–3 years through the employment of adaptive radiator designs in addition to providing thermal management for electrical and/or mechanical systems during extended periods of darkness such as lunar night.

Although the fuelling of a GPHS module with ^{90}SrO results in a 55.5% decrease in the module fuel mass, there is also a decrease in thermal output power by 82.9%. This ultimately requires almost 6 times the mass of ^{90}SrO fuel in order to achieve the same power thermal output as the GPHS RTGs fuelled by $^{238}PuO_2$. This translates into a 1.2 kg mass increase per module compared to the $^{238}PuO_2$ fuel mass. The dramatic increase in gamma radiation dose produced by such a substitution implies that increased shielding would be required which in turn could make the use of ^{90}Sr in the form of ^{90}SrO incompatible with he GPHS architecture. These findings are consistent with those presented in the study by Oandso et al. [45].

On completion of the initial GPHS study, it became apparent that several shielding criteria for reduced radiation power sources could be met by appropriate isotope selection. As indicated by the results in Table 2, the received neutron dose rate at a distance of 1 m from the centre of the current ^{238}Pu fuelled GPHS module is of the order of 0.1128 mSv/h (11.28 mRem/h). It is clearly possible to make alternative isotope power sources that have a dose rate that is at least an order of magnitude lower than current systems. This would have a dramatic impact on the applicability of RTGs over a greater range of space missions. The radiation dose to sensitive detectors would be reduced, increasing the operational lifetime of instruments [46]. The health and safety hazards for radiation workers and assembly technicians would also be reduced and/or may allow workers to work under occupational safety guidelines for longer periods of time with a given system. Planetary science missions with an astrobiology component and terrestrial studies designed to study ecosystems in extreme environments could benefit from reduced radiation power sources and isotopes that decay into stable daughters after a short period of time. By careful isotope selection, the effective sterilisation factor, and heat generated by the source can be minimised in order to ensure a reduced impact on the environment.

The current legal dose limit for radiation workers in the United Kingdom is 20 mSv per year, or under special cases this is set to a 100 mSv over a 5 year period where no more than a 50 mSv dose can be accumulated in a single year [47]. Based on these current guidelines and the above results from the MCNPX modelling, a radiation worker can work with oxygen-enriched $^{238}PuO_2$ fuelled GPHS modules for approximately 343 h per year. By making the substitution from oxygen-enriched $^{238}PuO_2$ fuel to oxygen-enriched $^{241}AmO_2$, it is possible for workers to spend a practically unlimited period each year working with GPHS modules. For the same electrical output power as current GPHS-RTGs, we would require around 90 modules fuelled with $^{241}AmO_2$ instead of 18 modules fuelled with $^{238}PuO_2$. This essentially means that workers must complete approximately five times the typical manual workload, but since there is little limitation to exposure time, the only penalty to the entire operation is in the form of the five times mass penalty for system heat sources. As can be deduced from Table 2, the decrease in dose rates and increase in recommended exposure times with the alternative isotope fuels, with the exception of ^{90}Sr, greatly outweighs any increase in manual workload for such substitution.

5. A laboratory breadboard model for low mass, reduced radiation RTGs

The overall RTG system power density is crucial for space and planetary science applications. A greater electrical power density ultimately translates into greater instrumentation or propellant mass for any given mission. For this reason, the systems and shielding configurations outlined in this study are designed to both minimise the radiation flux and to maximise the electrical power density.

Having selected ^{241}Am in the form of americium dioxide as the fuel for a long-lived laboratory scale low mass reduced radiation demonstration RTG (LMRR-RTG), a shielding configuration and cermet design was developed. The radiation fluxes for the various configurations were determine using the MCNPX [24] code. The shielding configuration that was derived to be most effective based on a tungsten encapsulated fuel cermets is illustrated in Fig. 13.

The central component to the system is the fuel cermet. As outlined in Section 6, the tungsten provides self-shielding against X-ray and gamma ray emission from the isotope source while ensuring the preservation of structural and thermal integrity of the radiological materials in the event of mission catastrophic failures such as launch aborts. A Boron loaded polyethylene casing is used to provide both neutron shielding and thermal insulation for the RTG system. The polyethylene content in the material thermalises the fast neutron emissions from the fuel source. The boron content is used to absorb, and hence attenuate the overall neutron flux while reducing the capture gamma ray production that would be produced in the same volume of polyethylene alone. The aluminium outer casing is the fourth and final component in the system configuration. This encloses the whole unit for mechanical integrity but also provides an outer layer of shielding against

Table 2
Alternative isotope study results for the replacement of the current PuO_2 fuel in the GPHS module

GPHS module fuel form	Pu-238 $^{238}PuO_2$ ceramic pellet	Am-241 $^{241}AmO_2$ (40 vol.%) and W (60 vol.%) cermet	Am-241 $^{241}AmO_2$ (50 vol.%) and W (50 vol.%) cermet	Am-241 $^{241}AmO_2$ ceramic pellet	Sr-90 ^{90}SrO ceramic pellet	Po-208 ^{208}Po (10 vol.%) and W (90 vol.%) cermet	Po-208 ^{208}Po (10 vol.%) and Al (90 vol.%) cermet	Po-210 ^{208}Po (10 vol.%) and W (90 vol.%) cermet	Po-210 ^{208}Po (10 vol.%) and Al (90 vol.%) cermet
Pellet mass (g)	1.88×10^2	2.66×10^2	2.54×10^2	1.91×10^2	8.3×10^1	2.99×10^2	5.50×10^1	2.99×10^2	5.50×10^2
Total fuel mass (g)	7.51×10^2	1.07×10^3	1.02×10^3	7.66×10^2	3.34×10^2	1.20×10^3	2.20×10^2	1.20×10^3	2.20×10^2
Change in module mass (g)	0	+314	+264	+14	−417	+445	−531	+446	−531
Pellet activity (Ci)	2.84×10^3	2.61×10^2	3.14×10^2	4.71×10^2	9.23×10^3	9.00×10^3	9.00×10^3	6.85×10^4	6.85×10^4
Change in pellet activity (Ci)	0	-2.58×10^3	-2.53×10^3	-2.37×10^3	$+6.39 \times 10^3$	$+6.16 \times 10^3$	$+6.16 \times 10^3$	$+6.80 \times 10^4$	$+6.80 \times 10^4$
Module activity (Ci)	1.13×10^4	1.04×10^3	1.26×10^3	1.88×10^3	3.69×10^4	3.60×10^4	3.60×10^4	$+2.74 \times 10^5$	$+2.74 \times 10^5$
Change in module activity (Ci)	0	-1.03×10^4	-1.00×10^4	-9.42×10^3	$+2.56 \times 10^4$	$+2.46 \times 10^4$	$+2.46 \times 10^4$	2.72×10^5	2.72×10^5
Module thermal power (W)	2.50×10^2	3.04×10^1	3.60×10^1	56.9×10^1	4.28×10^1	1.09×10^3	1.09×10^3	8.36×10^3	8.36×103
Change in Module thermal power (W)	0	-2.20×10^2	-2.14×10^2	-1.93×10^2	-2.07×10^2	$+8.36 \times 10^3$	$+8.36 \times 10^2$	$+8.33 \times 103$	$+8.33 \times 103$
Neutron dose rate at 1 m radius from GPHS (Sv/hr)	$6.534 \times 10^{-4} \pm 9.00 \times 10^{-6}$	$3.036 \times 10^{-5} \pm 7.94 \times 10^{-7}$	$3.788 \times 10^{-5} \pm 2.68 \times 10^{-7}$	$8.238 \times 10^{-5} \pm 1.86 \times 10^{-7}$	–	–	–	–	–
Neutron dose rate as a percentage of $^{238}PuO_2$ fuelled GPHS dose rate (%)	100	4.6	5.8	12.6	–	–	–	–	–
Gamma dose rate at 1 m radius from GPHS (Sv/hr)	$1.880 \times 10^{-6} \pm 1.09 \times 10^{-8}$	$6.882 \times 10^{-8} \pm 3.17 \times 10^{-10}$	$8.273 \times 10^{-8} \pm 2.79 \times 10^{-10}$	$1.740 \times 10^{-7} \pm 1.44 \times 10^{-9}$	$1.137 \pm 1.43 \times 10^{-2}$	–	–	–	–
Gamma dose rate as a percentage of $^{238}PuO_2$ fuelled GPHS dose rate (%)	100	3.7	4.4	9.3	6.0×10^5	–	–	–	–
Worker maximum recommended exposure time (hours per year)	31	657	527	242	0.018	>	>	>	>
Neutron dose rate at 1 m radius from GPHS fuelled with oxygen-enriched materials (Sv/hr)	$5.816 \times 10^{-5} \pm 1.14 \times 10^{-6}$	$6.162 \times 10^{-7} \pm 1.61 \times 10^{-8}$	$7.691 \times 10^{-7} \pm 5.44 \times 10^{-9}$	$1.672 \times 10^{-6} \pm 3.77 \times 10^{-9}$	–	–	–	–	–
Neutron dose rates for modules fuelled by oxygen-enriched materials as a percentage of the $^{238}PuO_2$ fuelled GPHS module dose rate (%)	100	1	1.3	3	–	–	–	–	–
Gamma dose rate at 1 m radius from GPHS module fuelled with oxygen-enriched materials (Sv/hr)	$1.673 \times 10^{-7} \pm 1.38 \times 10^{-9}$	$1.397 \times 10^{-9} \pm 6.44 \times 10^{-12}$	$1.679 \times 10^{-9} \pm 5.66 \times 10^{-12}$	$3.532 \times 10^{-9} \pm 2.91 \times 10^{-11}$	$1.137 \pm 1.43 \times 10^{-2}$	–	–	–	–
Gamma dose rates for modules fuelled by oxygen-enriched materials as a percentage of the oxygen-enriched $^{238}PuO_2$ fuelled GPHS module dose rate (%)	100	0.8	1	2	6.8×10^6	–	–	–	–
Worker maximum recommended exposure time to modules fuelled by oxygen-enriched materials(hours per year)	343	>	>	>	0.018	>	>	>	>

Data for oxygen-enriched oxides and oxides of natural oxygen composition is given for $^{238}PuO_2$ and $^{241}AmO_2$ fuelled modules. '>' Signifies that a practically unlimited annual exposure time is permissible.

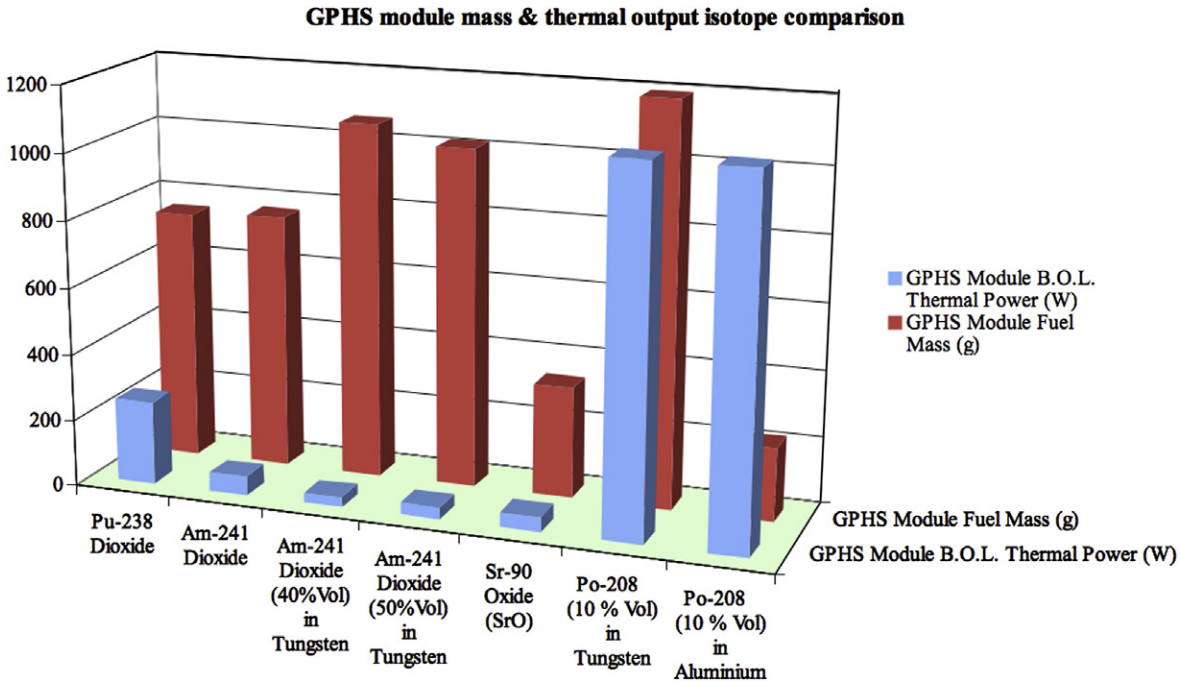

Fig. 11. A thermal performance and fuel mass comparison of substitute isotope candidates (excluding ^{210}Po) when used to fuel a GPHS module in contrast to the current performances of the GPHS modules fuelled by $^{238}PuO_2$.

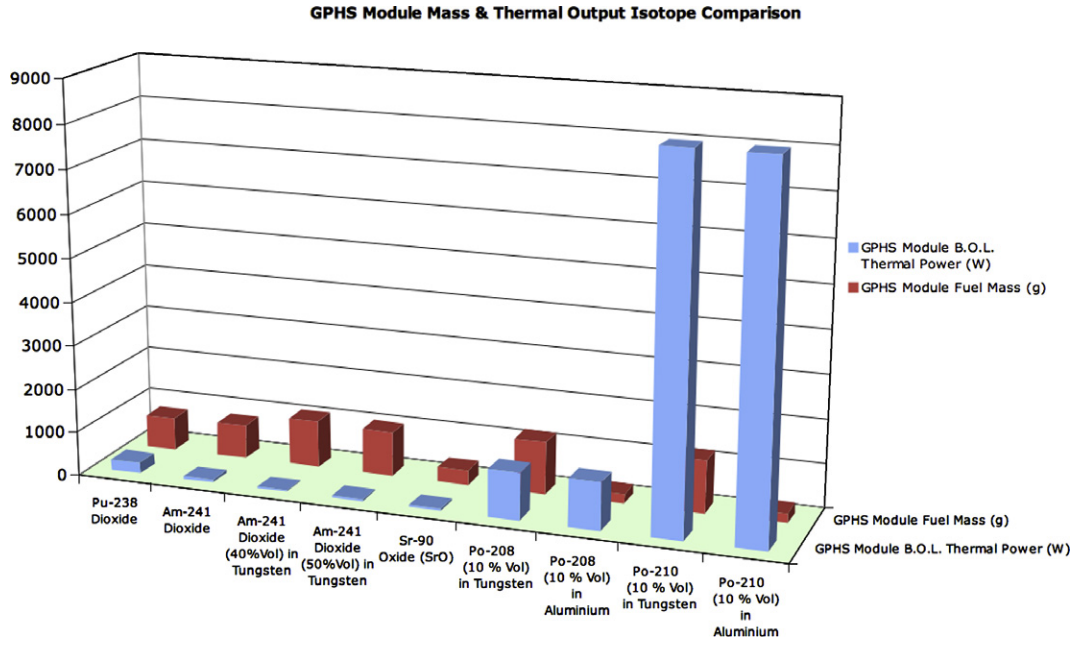

Fig. 12. A thermal performance and fuel mass comparison of all substitute isotope candidates when used to fuel a GPHS module in contrast to the performances of the GPHS modules fuelled $^{238}PuO_2$.

soft photon radiation. The thickness of each of the components in the shielding configuration was determined using the MCNPX [24] modelling technique.

This modelling focussed upon determining an optimum neutron shield thickness and was performed by modelling a source and a neutron shield in a spherical geometry. Three thicknesses of boron loaded polyethylene shielding (5 cm, 10 cm and 15 cm) were investigated and the photon and neutron dose rates tallied in a 1 cm thick shell of water at a radius of 1 m from the source. The composition of the ^{241}Am source was also set as a variable so as to investigate its effect on the overall mass of the assembly. The source was presented in oxide form ($^{241}AmO_2$) or encapsulated in tungsten as a cermet, the volumetric composition of which was either 40% or 50% $^{241}AmO_2$. In order to provide comparison, $^{238}PuO_2$ was also modelled within identical configurations. The oxygen composition within the oxide compounds of both PuO_2 and AmO_2 was set as another variable in order to determine the effect of oxygen-enrichment upon the shielding requirements. Thermal power output levels of between 10 and 200 W were also set as the third variable for the investigation. The source emission

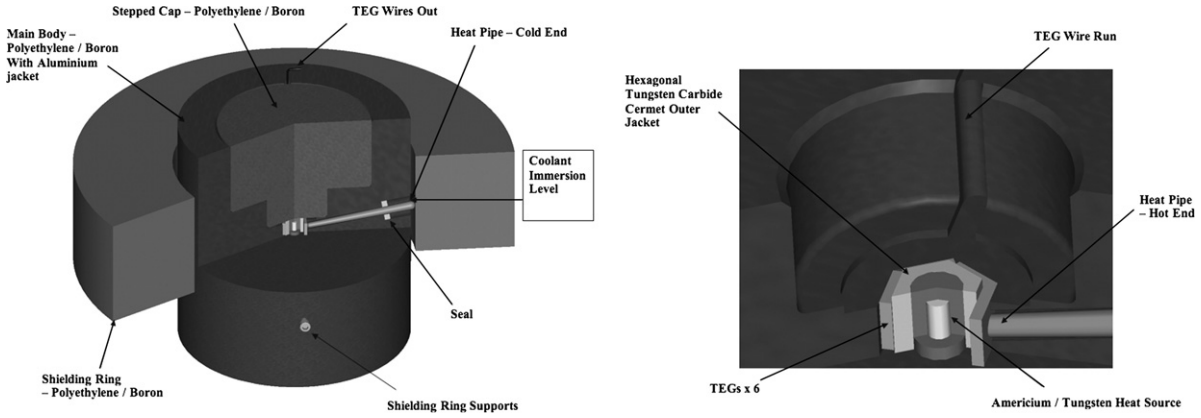

Fig. 13. Schematic of the laboratory breadboard model of a low mass, reduced radiation (LMRR)-RTG demonstration model.

spectra were defined as in Section 2. Each specific configuration was simulated in MCNPX Version 6c [24], each simulation terminating after a total of $1x10^6$ source particles had been tracked through the geometry.

For oxide sources with natural oxygen composition, it was determined that $^{241}AmO_2$ sources surrounded by a 5 cm thick boron loaded polyethylene (B.L.P.E.) shield resulted in approximately the same neutron dose rates as for $^{238}PuO_2$ surrounded by a 10 cm thick B.L.P.E. shield for the thermal power range between 0 and 200 W. This is illustrated in Fig. 14. Fig. 15 illustrates the associated masses that are observed with this shielding configuration. Over the identical thermal power range for oxygen-enriched sources, the dose rates that were observed for an unshielded $^{241}AmO_2$ source were approximately equal to those of $^{238}PuO_2$ sources surrounded by a 15 cm thick B.L.P.E. shield (Fig. 16). This marked difference in shielding requirements is due to the domination of spontaneous fission derived neutron yields for the oxygen-enriched materials and the difference between the spontaneous fission probabilities of ^{241}Am and ^{238}Pu. Fig. 17 illustrates the masses of these configurations for the oxygen-enriched sources.

What is particularly evident in these results is that for any given power level, for an equal neutron dose rate to be exhibited by both oxygen-enriched americium and plutonium systems, the total masses of the ^{238}Pu configurations is approximately 10 times greater than those for ^{241}Am. This is an extremely important factor that must be considered during isotope selection for power sources where potential radiation exposure to workers or during launch failure scenarios is to be minimised.

Based upon the safety rationale for tungsten encapsulation and on the neutron dose reductions from the results above, a final configuration for a 5 W_e prototype breadboard model for low mass,

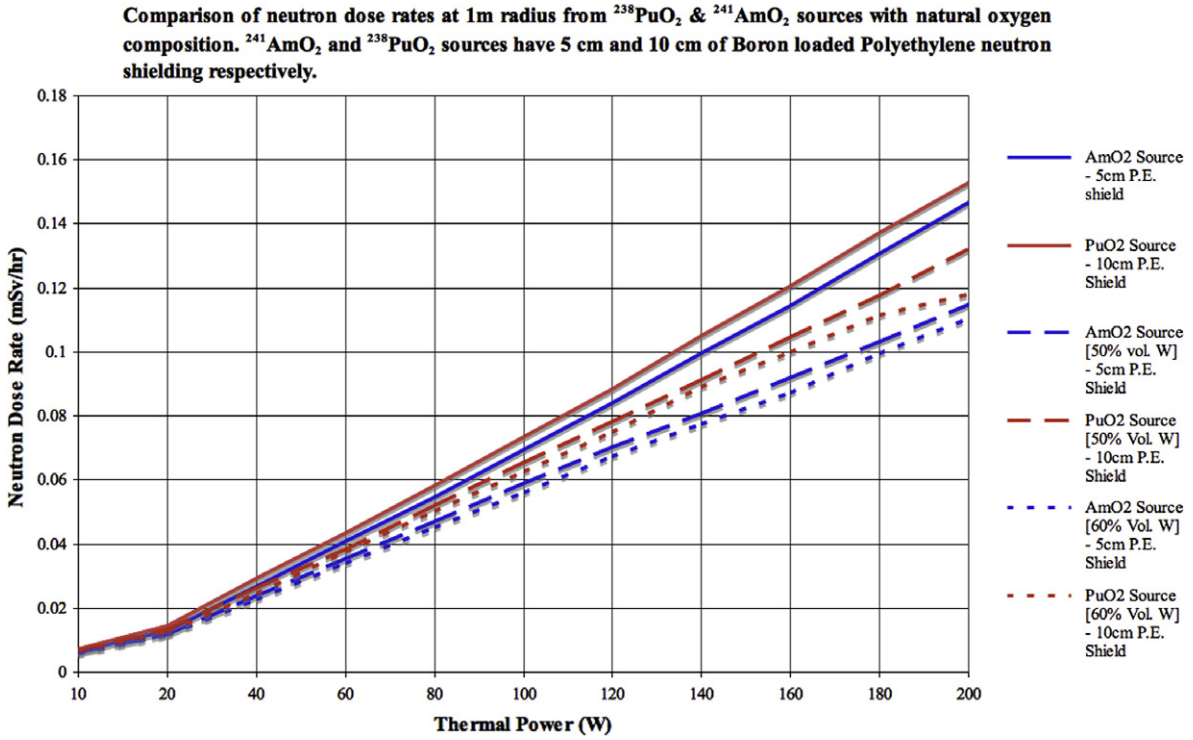

Fig. 14. Comparison of MCNPX [24] derived results for the dose rates of modelled systems fuelled by $^{241}AmO_2$ (natural oxygen composition) in oxide form and in tungsten based cermets relative to those of devices with similar dose rates fuelled by $^{238}PuO_2$ (natural oxygen composition) in oxide form and tungsten cermets. These system masses are illustrated as a function of source thermal output power and dose rate equivalence. The tungsten volume fraction for cermet-based sources are listed in the key.

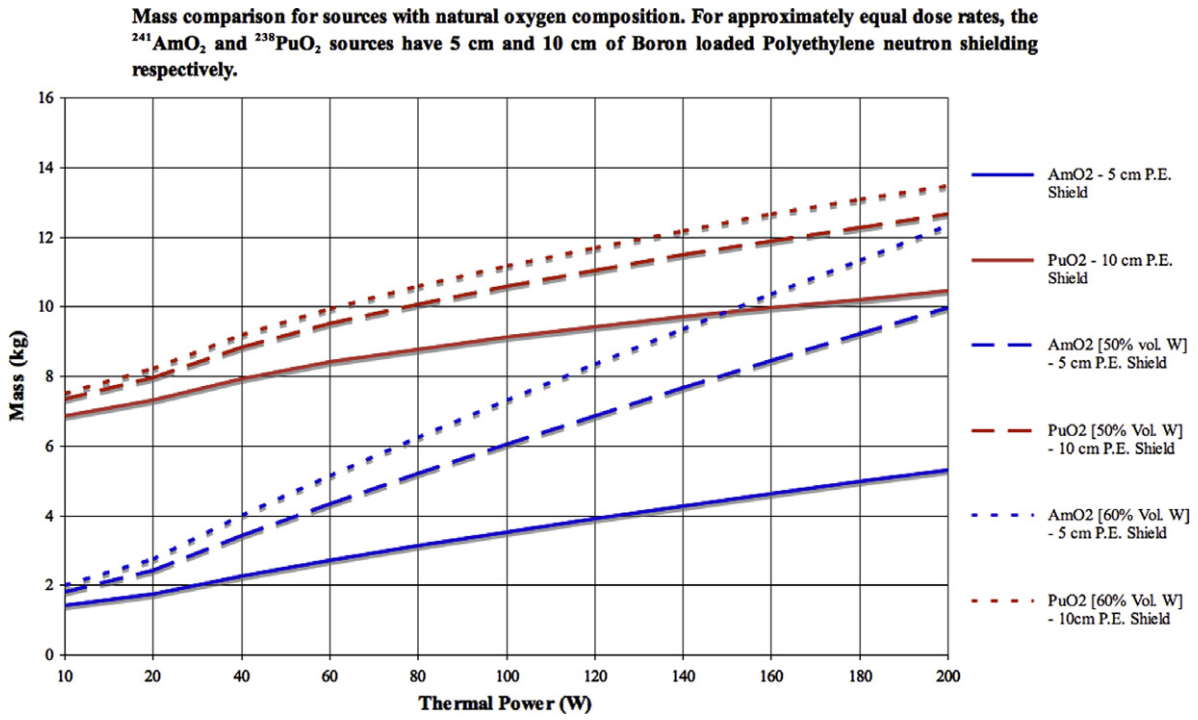

Fig. 15. Comparison of MCNPX [24] derived results for the masses of modelled systems fuelled by $^{241}AmO_2$ (natural oxygen composition) in oxide form and in tungsten based cermets relative to those of devices with similar dose rates fuelled by $^{238}PuO_2$ (natural oxygen composition) in oxide form and tungsten cermets. These system masses are illustrated as a function of source thermal output power and dose rate equivalence. The tungsten volume fraction for cermet based sources are listed in the key.

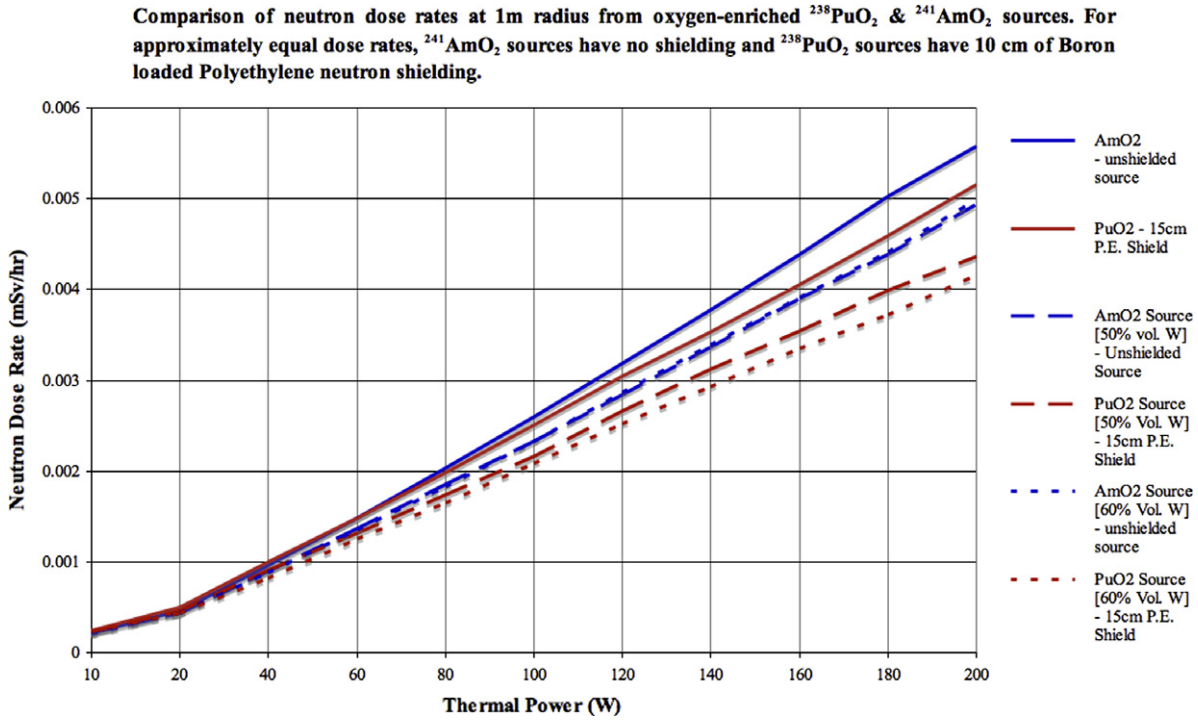

Fig. 16. Comparison of MCNPX [24] derived results for the dose rates of modelled systems fuelled by oxygen-enriched $^{241}AmO_2$ in oxide form and in tungsten based cermets relative to those of devices with similar dose rates fuelled by oxygen-enriched $^{238}PuO_2$ in oxide form and tungsten cermets. These system masses are illustrated as a function of source thermal output power and dose rate equivalence. The tungsten volume fraction for cermet based sources are listed in the key.

reduced radiation RTGs was assigned. It should be noted that optimum configurations for neutron shielding masses can only be achieved through the enrichment of the ^{16}O content of the americium oxide. For the purpose of the laboratory scale breadboard prototype, mass optimisation is not essential but demonstration of such principals will be made for an AmO_2 source with a natural oxygen composition. The physical properties of the concept breadboard prototype system are listed in Table 3.

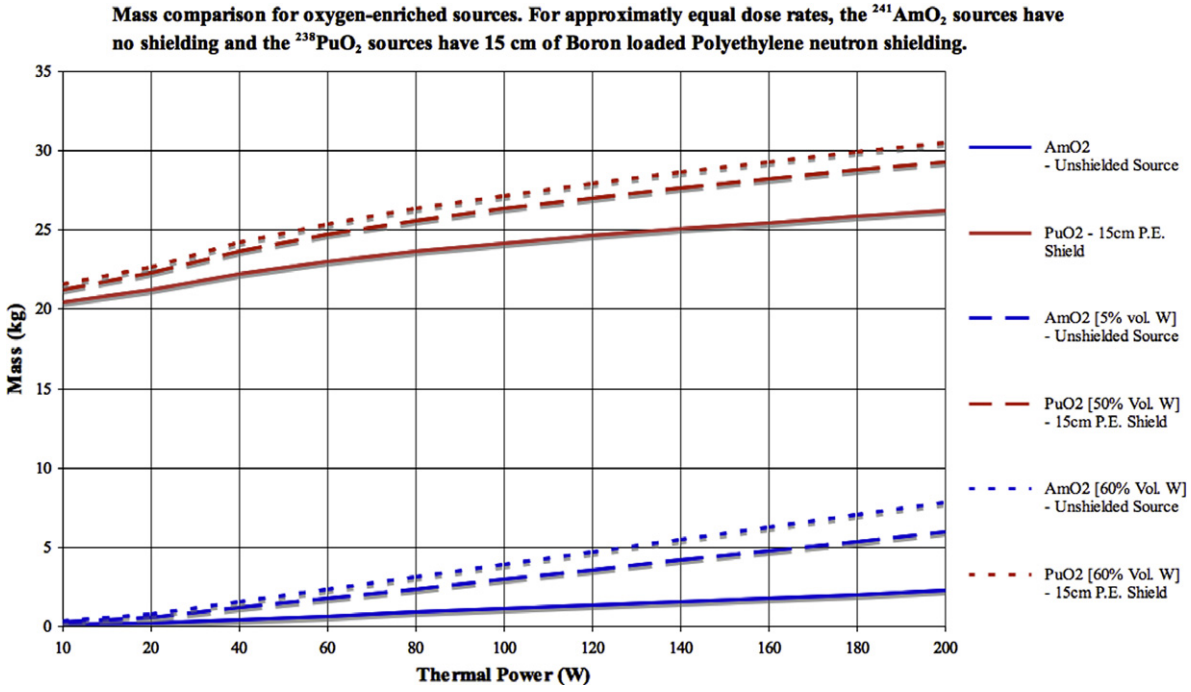

Fig. 17. Comparison of MCNPX [24] derived results for the masses of modelled systems fuelled by oxygen-enriched $^{241}AmO_2$ in oxide form and in tungsten based cermets relative to those of devices with similar dose rates fuelled by oxygen-enriched $^{238}PuO_2$ in oxide form and tungsten cermets. These system masses are illustrated as a function of source thermal output power and dose rate equivalence. The tungsten volume fraction for cermet based sources are listed in the key.

Table 3
Physical properties of 5 W_e prototype breadboard model for a low mass reduced radiation RTG

Prototype breadboard model for low mass, reduced radiation RTG physical properties	
Thermal output power (W_t)	100
Electrical output power (W_e) (based on 5% conversion efficiency)	5
Fuel form	Americium-241 tungsten cermet 50% $^{241}AmO_2$: 50% W (natural oxygen composition $^{241}AmO_2$ oxide)
Neutron shielding	5 cm Thick boron loaded polyethylene (B.L.P.E.)
1 m neutron dose rate (Sv/hr)	6.7×10^{-5}
1 m photon dose rate (Sv/hr)	2.8×10^{-7}
Total system mass (kg)	6.4

Having derived the optimum radiation shielding configuration above, the thermal environment for the system was evaluated using a finite element modelling (FEM) and analysis package produced by Ansys Inc. [48]. In the FEM simulations, for the purpose of the laboratory scale demonstration model, the external temperature of the system was held at the carbon dioxide sublimation temperature of −80 °C by a working fluid. Heat pipes were added to the model so as to ensure that an appropriate temperature gradient was maintained across the thermoelectric generators. The optimum temperature gradient across the junction for the current design was determined to be 150 °C. The heat extraction power by the heat pipe system was selected so that the heat source cannot not exceed 60% of the melting temperature of the boron loaded polyethylene neutron shielding, which is approximately 120 °C. This was done to prevent structural deformation of the device. By ensuring that the converter cold side temperature was below −30 °C, this optimum temperature gradient could be achieved while preventing the internal temperature from exceeding the melting temperature of the polyethylene shielding.

6. Conclusions and future work

Through the comparison of isotopes made in Section 2, we have identified three isotopes that can deliver suitable power densities for space missions while reducing the radiation doses delivered by such sources. The factor that drives selection from these isotopes is the mission architecture. ^{208}Po and ^{210}Po are best suited to missions requiring short durations of thermal and/or electrical power before decaying into stable isotopes of lead. Such missions include melt-penetration of icy planetary surfaces while minimising the overall impact upon the environment. The use of the polonium isotopes implies a high initial thermal loading in order to account for the isotopes' short half-life, which in turn demands adaptive radiator or heat pipe design for steady state electrical power output.

^{241}Am has a half-life that is approximately five times greater than that of ^{238}Pu. We have determined that an $^{241}AmO_2$ source neutron yield is approximately an order of magnitude lower than a $^{238}PuO_2$ source of equal mass and degree of ^{16}O enrichment. We have also demonstrated that shielded heat sources fuelled by oxygen-enriched $^{238}PuO_2$ have masses that are up to 10 times greater than those fuelled by oxygen-enriched $^{241}AmO_2$ with equivalent thermal power outputs and neutron dose rates at 1 m radii. For these reasons, ^{241}Am is well suited to missions that demand long duration power output from a power supply, such as deep spaceflight missions and similar missions that use instrumentation and electronics systems that are sensitive to or are susceptible to neutron radiation damage.

Our theoretical research has shown that isotope encapsulation within cermet matrices has many safety benefits. In order to verify cermet production techniques, a collaborative program has been established between the University of Leicester Space Research Centre, University of Leicester Department of Engineering and the Center for Space Nuclear Research at Idaho National Laboratory. The results from the experimental research program will be published in a later paper.

Acknowledgements

Engineering and Physical Sciences Research Council (EPSRC) for funding the project (EP/D030277/1). Mike Evans and Tim Stevenson – University of Leicester. Darryl. Butt – Boise State University.

References

[1] E. Levnor, I. Linkov, J.M. Proth, Strategic Management of Marine Ecosystems, Springer, 2005. p. 21, ISBN 1-4020-3158-0.
[2] Office of Polar Programs Environment Section, Environmental Action Memorandum (Installation, Maintenance and Removal of Automatic Weather Stations in Antarctica), OPP opp93102 (202/357-7766), 18th February 1993.
[3] V.P. Chechev, N.K. Kuzmenko, Table of Radionucleides, vol. 2., BNM-LNHB/CEA – Monographie Bureau International Des Poids Et Mesures BIPM-5, 2004.
[4] Department of Energy, Draft Environmental Impact statement for the proposed Consolidation of Nuclear Operations related to Production of Radioisotope Power Sytems, DOE/EIS-0373D, p. 19.
[5] G.L. Bennett, Space nuclear power: opening the final frontier, in: Fourth International Energy Conversion Engineering Conference and Exhibit (IECEC) 26–29 June 2006, San Diego, California AIAA, 2006-4191.
[6] J.A. Angelo, D. Buden, Space Nuclear Power, Orbit Book company Inc. ISBN: 0-89464-000-3.
[7] Courtesy of the NASA Apollo 16 Lunar Surface Journal Image Library.
[8] C.E. Kelly, MHW RTG performance during LES 8/9 and voyager missions. New Mexico Univ. in: Transactions of the Fourth Symposium on Space Nuclear Power Systems, 1987, p. 197 (N88-24254 17-73).
[9] G.L. Bennett, J.J. Lombardo, R.J. Hemler, G. Silverman, C.W. Whitmore, W.R. Amos, E.W. Johnson, A. Schock, R.W. Zocher, T.K. Keenan, J.C. Hagan, R.W. Englehart, Mission of daring: the general purpose heat source radioisotope thermoelectric generator, in: Fourth International Energy Conversion Engineering Conference 26th–29th June 2006, AIAA 2006-4096.
[10] C.P. Bankston, K.L. Atkins, E.F. Mastal, D.G. McConnell, Acta Astronaut. 24 (1991) 161. doi:10.1016/0094-576(91)90163-Y.
[11] Y. Zhamd, G. Zeng, R. Singh, J. Christofferson, E. Croke, J.E. Bowers, A. Shakouri, Measurement of Seebeck coefficient perpendicular to SiGe superlattice, Thermoelectrics, 2002. in: Proceedings ICT '02. Twenty-First International Conference on Thermoelectrics (Cat. No.02TH8657), p. 329.
[12] J. Kaye, J.A. Welsh, Direct Conversion of Heat to Electricity, John Wiley, 1960.
[13] G. Miskolczy, D.P. Lieb, Radioisotope thermionic converters for space applications, in: Proceedings of the 25th Intersociety Energy Conversion Engineering Conference, IECEC-90, vol. 1, p. 222. ISBN: 0-8169-0490-1.
[14] C.S. Murray, C.J. Crowley, S. Murray, N.A. Elkouh, R.W. Hill, D.E. Chubb, Thermophotovoltaic converter design for radioisotope power systems, in: AIP Conf. Proceedings 738, 2004, p. 123 doi:10.1063/1.1841887.
[15] D.J. Anderson, W.A. Wong, K.L. Tuttle, An overview and status of NASA's radioisotope power conversion technology NRA, NASA/TM-2005-213980.
[16] P.C. Schmitz, L.B. Penswick, R.K. Shaltens, A design of a modular GPHS-Stirling power system for a lunar habitation module, NASA/TM-2005-213991, AIAA-2005-5716.
[17] L.S. Mason, J.G. Schreiber, A historical review of Brayton and Stirling power conversion technologies for space applications, in: Proceedings of the Space Nuclear Conference 2007, Boston Massachusetts. June 24-28 2007, Paper 2034, American Nuclear Society, ISBN: 0-89448-053-7.
[18] T.S. Balint, J.F. Jordan, Acta Astronaut. 60 (2007) 992.
[19] Knolls Atomic Power Laboratory Inc., Chart of the Nuclides, 16th Ed., Lockheed Martin, 2002.
[20] F. Asaro, S.G. Thompson, I. Perlman, Phys. Rev. 92 (3) (1953) 694.
[21] Argonne National Laboratory Environmental Science Division (EVS), Curium Human Health Fact Sheet, August 2005.
[22] US Department of Energy, Processes and characteristics of major isotopes handled at mound, 1993.
[23] P.E. Figgins; The Radiochemistry of Polonium, National Academy of Sciences National Research Council Nuclear Science Series NAS-NS 3037, 1961.
[24] MCNP – a general Monte Carlo n-particle transport code, version 5. X-5 Monte Carlo Team. LA-UR-03-1987. Los Alamos National Laboratories, Los Alamos, New Mexico, 2003.
[25] W. Gruhle, T.H. Bauer, T.H. Seligmann, H.H. Hackenbroich, Z. Phys. (1973).
[26] V.A. Vukolov, F.E. Chukreev, Evaluated (A,N) reaction data on most important nuclei entered in composition of chemical reagents which used in nuclear fuel work process. J,VAT/O,4,31,1983 Voprocy Atomnoy Nauki i Tekhniki, Seriya Obshch, 1983.
[27] T. Murata, K. Shibata, JENDL (alpha,n) Reaction Data File 2003, Japanese Evaluated Nuclear Data Library, Japan Atomic Energy Agency, (JENDL-AN-2003).
[28] M. Stanley-Livingston, H.A. Bethe, Rev. Mod. Phys. 9 (1937) 245. doi:10.1103/RevModPhys.9.245.
[29] R.M. Ambrosi, J.I.W. Watterson, B.R.K. Kala, Nucl. Instrum. and Meth. B 139 (1998) 286.
[30] H. Matsunobu, T. Oku, S. Iijima, Y. Naito, F. Masukawa, R. Nakasima, Data Book for Calculating Neutron Yields from (α, n) Reaction and Spontaneous Fission, Japan Atomic Energy Research Institute, Tokai mura, Naka gun, Ibaraki ken, 1992. JAERI 1324.
[31] W.B. Wilson, R.T. Perry, W.S. Charlton, T.A. Parish, E.F. Shores, Radiat. Prot. Dosim. 115 (14) (2005) 117.
[32] O.L. Kruger, Process of making oxygen enriched plutonium dioxide (PuO_2), United States Patent 4,042,670.1977 August 16.
[33] D.L. Plymale, J. Inorg. Nucl. Chem. 30 (1968) 886.
[34] S.D. Howe, N. Barra, J. Bess, E. Colvin, P. Cummings, B. Cunningham, M. Ghrist, R. Johnson, R. O'Brien, J. Perkins, K. Supak, M. Yaho, Returning humans to the moon: comparison of chemical Engine and nuclear rocket performance as an earth departure stage, in: Proceedings of Space Nuclear Conference 2007, Boston Massachusetts, June 24–28 2007, American Nuclear Society, ISBN: 0-89448-053-7.
[35] S.K. Borowski, R.R. Corban, Nuclear thermal rocket/Vehicle design options for future NASA missions to the moon and mars, AIAA-93-4170, 1993.
[36] T.W. Knight, S. Anghaie, J. Nucl. Mater. 306 (2002) 54.
[37] D.A. Seifert, R.L. Stuart, P.K. Conn, H.W. McLaughlin, G.J. Luersen, Fission product behavior within two W–UO_2 cermet fuel elements irradiated in a temperature gradient. Nuclear Space Programs Space Systems, General Electric, Cincinnati, Ohio, 1968.
[38] X. Wang, Y. Xie, H. Guo, O. Van der Biest, J. Vleugels, Rare Metals 25 (3) (2006) 246.
[39] H.V. Atkinson, S. Davies, Metall. Mater. Trans. A 31 (12) (2000) 2981.
[40] C.C. Jia, H. Tang, X.Z. Mei, F.Z. Yin, X.H. Qu, Mater. Lett. 59 (2005) 2566.
[41] M. Rosinski, E. Fortuna, A. Michalski, Z. Pakiela, K.J. Kurzydiowski, Fusion Eng. Design (2007), doi:10.1016/j.fusengdes.2007.06.017.
[42] R.M. Ambrosi, H.V. Atkinson, N.P. Bannister, D.P. Butt, J. Pan, Materials world network: cermet encapsulation at very high temperatures using field assisted sintering, proposal to the National Science Foundation for program announcement NSF 07-574, 13th November 2007.
[43] J. Zhang, T. Wu, L. Wang, W. Jiang, L. Chen, Compos. Sci. Technol. 68 (2008) 499.
[44] M. Zadra, F. Casari, A. Molinari, Mater. Sci. Forum 534–536 (2007) 1401.
[45] California Institute of Technology Jet Propulsion Lab (JPL), Cassini Program environmental impact study volume 2: Alternate Mission and Power Supply, JPL Publication No. D-11777. Cassini document No. 699-070-2, 1994.
[46] J.E. Brau, O. Igonkina, C.T. Potter, N.B. Sinev, Nucl. Instrum. and Meth. B Phys. Res. A 549 (2005) 117.
[47] United Kingdom Health and Safety Executive, Ionising Radiation Regulations, 1999 – (IRR99).
[48] Ansys Finite Element and multi-physics analysis software package, Ansys Inc, Canonsburg PA, USA.